Journal of Physics and Chemistry of Solids 159 (2021) 110278

Contents lists available at ScienceDirect

Journal of Physics and Chemistry of Solids

journal homepage: www.elsevier.com/locate/jpcs

Structural, morphological and magnetic properties of Ni/NiO systems produced by a sorbitol-assisted wet chemical method

A.J. Freitas Cabral [a,*], Lorena Nascimento [b], X. Gratens [c], V.A. Chitta [c], Waldomiro Paschoal Jr. [b,**], C.M. Rocha Remédios [b]

[a] Universidade Federal do Oeste do Pará (UFOPA), Santarém, PA, Brazil
[b] Instituto de Ciências Exatas e Naturais, Universidade Federal do Pará (UFPA), Belém, PA, Brazil
[c] Instituto de Física, Universidade de São Paulo, São Paulo, SP, Brazil

ARTICLE INFO

Keywords:
Ni/NiO systems
Sorbitol
Wet chemical
Magnetic properties

ABSTRACT

In this work, we show the sorbitol-assisted synthesis method to produce polycrystalline Ni/NiO systems with different phase proportions. The samples were prepared from heat treatment of an aqueous solution of nickel chloride and sorbitol by using a simple wet chemical approach. The produced samples were calcined at 500 °C and the characterization of the as-produced samples was performed by X-ray diffraction (XRD), Rietveld analysis and scanning electron microscopy (SEM). Magnetic properties of Ni/NiO samples were investigated by DC magnetometry technique. XRD data reveal an increase in the proportion of metallic Ni phase in the synthesis products as the quantity of sorbitol in the starting solution is increased. Multi-phase Rietveld analysis showed that the phase fractions in the samples varied from 5.9 wt% (94.1 wt%) to 22.5 wt% (77.5 wt%) for Ni (NiO) phase. SEM analyses show changes in particle shape and size when sorbitol increases. The increase in the magnetization with increasing of Ni phase content up to at 65 kOe is assigned to the increase of the ferromagnetic (FM) phase.

1. Introduction

The interest in the synthesis of two-phase magnetic systems of the metal-metal oxide type has drawn much attention because they exhibit interesting magnetic properties and interface effects [1]. In general, the synthesis of two-phase compounds with controlled composition of their constituents is a requirement for technological applications. An important metal-metal oxide system is the Ni/NiO since it is used to investigate exchange bias effects and presents catalytic properties [2]. The Ni/NiO system has been produced by several synthesis routes and in the form of bilayer thin films, core-shell nanoparticles, and nanocomposites [3–5].

Wet chemical methods that follow liquid-phase routes, such as sol-gel and polyol process are widely used for synthesis of metal oxide and metal polycrystalline materials, respectively [6,7]. In the oxide synthesis via aqueous sol-gel process based on the approach of metal salts, the use of organic chelating (complexing) agents is rather common, because they help to reduce free ions in the aqueous solution forming metal complexes and favor the gel formation [8]. Whereas in the synthesis of metal particles by polyol process, the polyalcohols act as reducing agents and reaction medium [9]. Therefore, the combination of both sol-gel and polyol process can be useful for the synthesis of metal-metal oxide system by adjustment of hydrolysis ratio, which is the water to metal molar ratio [10].

Sorbitol is a sugar alcohol and it has been used as a complexing and chelating agent for synthesis of oxide materials [11,12] and as well as a reducing agent of copper in the process of laser-induced chemical liquid phase deposition [13]. It is known from literature that organic chelating (complexing) agents, in some cases, act as reducing agents (ref. [14] and references therein). So, sorbitol becomes an attractive candidate for the synthesis of metal-metal oxide systems in aqueous solution.

Despite the numerous reports on the synthesis of Ni/NiO systems [2–5,15,16], there are few describing the use of nickel(II) chloride as a precursor and, to our knowledge, none published using a sorbitol-assisted wet chemical method. Therefore, it is important to produce the Ni/NiO systems by a simple and inexpensive preparation

* Corresponding author.
** Corresponding author.
E-mail addresses: alex.cabral@ufopa.edu.br (A.J.F. Cabral), wpaschoaljr@ufpa.br (W. Paschoal).

https://doi.org/10.1016/j.jpcs.2021.110278
Received 12 April 2021; Received in revised form 17 June 2021; Accepted 17 July 2021
Available online 21 July 2021

Table 1
Synthesis conditions.

Sample	Water (ml)	Nickel Chlo-ride (mg)	Sorbitol (ml)
S10	20	2.38	10
S20	20	2.38	20
S25	20	2.38	25

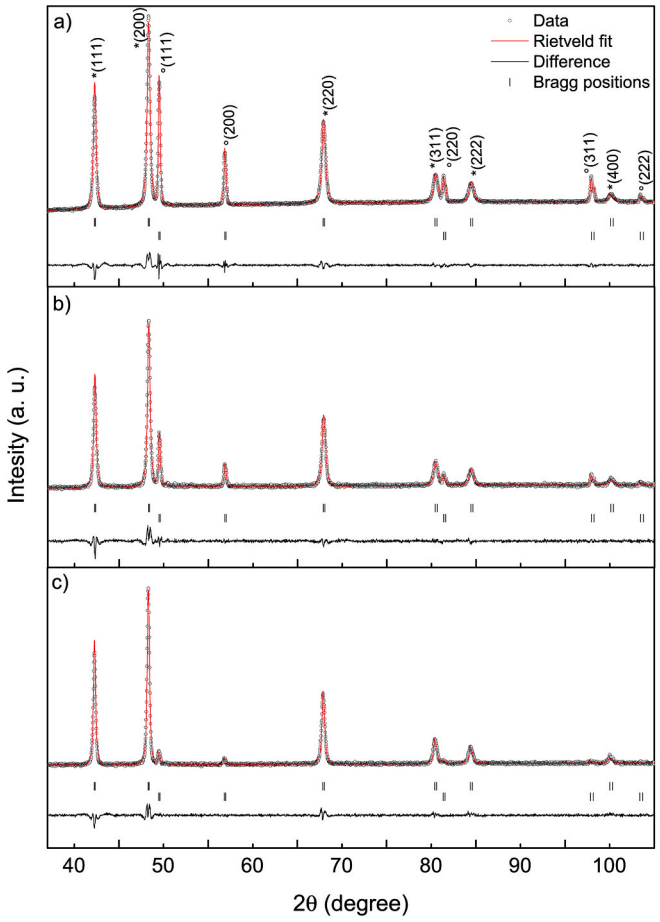

Fig. 1. Rietveld analysis of XRD patterns for samples S25 (a), S20 (b) and S10 (c). The positions of the NiO and Ni Bragg peaks are presented by uper and lower double vertical lines, respectively.

process using alternative reagents.

Taking into account the fact that sorbitol presents both roles, of chelating and reducing agent, our primary focus is to produce polycrystalline Ni/NiO samples at different proportions of their constituents by a wet chemical approach using nickel(II) chloride. In the sequence we want to study the influence of sorbitol amount in the starting solution on the proportion of the crystalline phases, microstructures, particle size, particle morphology, and magnetic properties of the produced samples.

2. Experiments

To synthesize polycrystalline Ni/NiO samples by a wet chemical route, we used nickel chloride hexahydrate ($NiCl_2{\cdot}6H_2O$, 99.9%, VETEC) and sorbitol ($C_6H_{14}O_6$, 70% (w/w), Synth) as starting materials. A proper amount of solid nickel chloride was dissolved in 20 ml of distilled water at 50 °C, under constant stirring until its total dissolution. Afterward, appropriate amounts of 70% sorbitol aqueous solution (10, 20, and 25 ml) were added to nickel chloride aqueous solutions and these solutions were vigorous mixed for 15 min, until a homogeneous and highly viscous solutions were obtained. In order to eliminate residual solvent and to reach out gels, the obtained resulting solutions were led in an oven at 75 °C for 24 h. Green gels were formed and they were thermally treated at 500 °C for 3 h under air atmosphere. The obtained samples were termed S10, S20, and S25, which correspond to sorbitol amounts used. The synthesis parameters, namely distilled water, nickel chloride, and sorbitol quantity are depicted in Table 1.

The crystalline phase identification of the as-produced samples was carried out at room temperature by X-ray diffraction (XRD) technique, through a Bruker D8 Advance diffractometer by using CuKα radiation (λ = 1.54056 Å). The XRD data were collected over 2θ varying from 20° to 120°, step size of 0.02, and acquisition time of 60 s. The phase quantification and microstructure properties of Ni/NiO samples were determined by Rietveld refinement by using the program *Fullprof* [17]. The morphological properties of the obtained Ni/NiO systems were investigated by scanning electron microscopy (SEM). Scanning electron micrographs of the produced samples were acquired on a Tescan Vega-3 scanning electron microscope. Ni/NiO samples were placed on metal/-glass plate. In order to avoid electric charging and to obtain good SEM images a thin (20 nm) gold/palladium film was deposited, by sputtering, on the Ni/NiO samples and 15 kV acceleration energy and low electron beam intensity were used. DC Magnetic properties, such as magnetization as a function of temperature and magnetic field were performed in a superconducting quantum interference device (SQUID–Cryogenic S600).

3. Results and discussion

3.1. Crystal structure analysis, phase quantification, and microstructure

Fig. 1 shows the XRD patterns of S10, S20 and S25 samples, which are in agreement with the literature about Ni–NiO crystalline materials

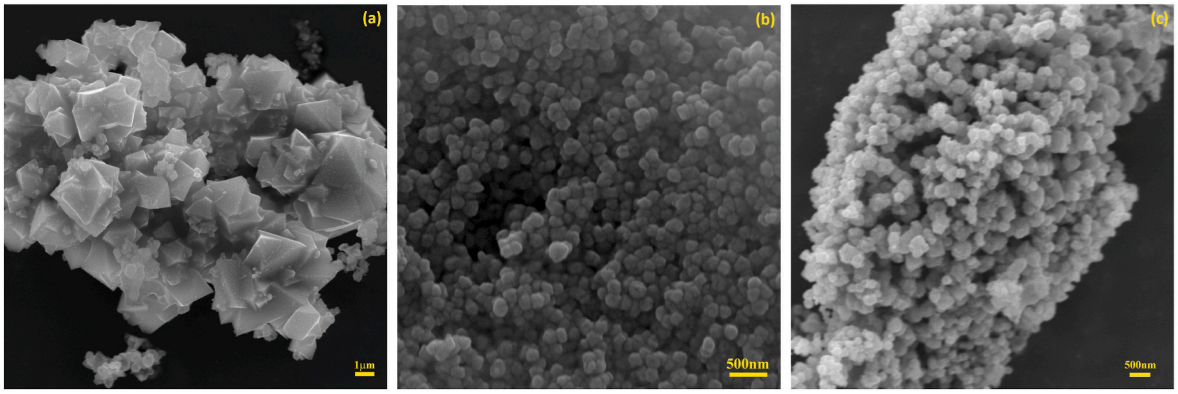

Fig. 2. Scanning electron micrographs of the samples S10 (a), S20 (b) and S25 (c).

Table 2
Results obtained from Rietveld refinement of XRD data. Lattice parameters, phase fractions, microstructures, R-factors, and goodness of fit.

Parameters	S10	S20	S25
NiO phase			
Lattice constant (Å)	4.179(5)	4.177(4)	4.176(2)
Phase fraction (wt%)	94.1(1.1)	86.9(1.2)	77.5(6)
D (nm)	43.3(0)	28.0(0)	27.7(0)
ε (%%)	12.9(0)	9.6(0)	24.3(0)
Ni phase			
Lattice constant (Å)	3.526(4)	3.524(3)	3.524(2)
Phase fraction (wt%)	5.9(4)	13.1(3)	22.5(2)
D (nm)	25.7(0)	36.5(0)	42.0(0)
ε (%%)	–	–	–
R_p - R_{wp}	3.37–4.39	3.20–4.19	1.91–2.69
χ^2	1.27	1.26	2.53

[5,18,19]. The diffraction peaks can be indexed to cubic Ni and cubic NiO phases. The characteristic peaks of NiO phase, indicated by (*), are indexed to the (111), (200), (220) (311), (222) and (400) planes. Whereas the diffraction peaks of Ni phase, denoted by ( ), are assigned to the (111), (200), (220), (311) and (222) planes. The evolution of the reflection from the (111) plane of Ni phase shows a clear increase in Ni phase content from S10 to S25 sample, as can be observed in Fig. 1a–c. This increase in Ni phase content is related to the increase of sorbitol amount used in precursor solution, since the sorbitol amount was the only variable parameter in the synthesis process. It is worth mentioning that single-phase NiO was achieved using 5 ml of sorbitol in the starting solution. It is known from literature that the main chemical reactions in the sol-gel and polyol process are hydrolysis and reduction, respectively [6,7]. Thus, a proposal for the synthesis of Ni/NiO samples and the increase of Ni fraction in the samples is given as follow: in our synthesis process both hydrolysis and reduction chemical reaction can occur, because the samples are composed of both metal and metal oxide, as determined from XRD data. This suggests that the sorbitol in the aqueous medium acts as chelating agent because it avoids the growth of particles (see Fig. 2) as well as reducing agent because it favors the formation of metallic Ni phase in the samples. As the sorbitol amount is enhanced, the hydrolysis is more and more inhibited, so more free Ni^{2+} ions in the solution are reduced to Ni^0, driving to increase of Ni fraction in the samples. The synthesis route used here can be compared that proposes by L. Poul et al. [10], in which the formation of metal or oxide particle is adjusted by absence or presence of water, respectively. However, here the fraction of metal and metal oxide phase is tailored by sorbitol amount.

The multiphase Rietveld refinement was used to quantify each phase in the samples. XRD patterns were refined assuming a cubic crystal system and space group $Fm\bar{3}m$ for Ni (ICDD-pdf card 86–1518) and NiO (ICDD-pdf card 72–1832) phases. The refined parameters were background, scale factor, unit cell constants, peak profile parameters, and atomic displacement parameters. The atomic coordinates and occupancy factors of both phases were kept fix during all the refinement. The lattice parameters, phase fractions, and reliability indices weighted-profile R-factor (R_{wp}), profile R-factor (R_p), and goodness of fit (χ^2) extracted from Rietveld analysis are provided in Table 2. The lattice parameter values for Ni and NiO phases for all samples are consistent with values reported in literature [5]. The Ni phase fraction increased from 5.9 wt% to up 22.5 wt% and NiO phase fraction decreased from 94.1 wt% down to 77.5 wt% with increasing of sorbitol volume. The small reliability indices indicated that the samples are composed of cubic Ni and cubic NiO.

Information about the microstructures such as diffraction domain (D) and microstrain (ε) were evaluated by X-ray line profile analysis using the methodologies described by *Fullprof* [20]. The diffraction peak broadening due to instrument contributions was determined by Le Bail

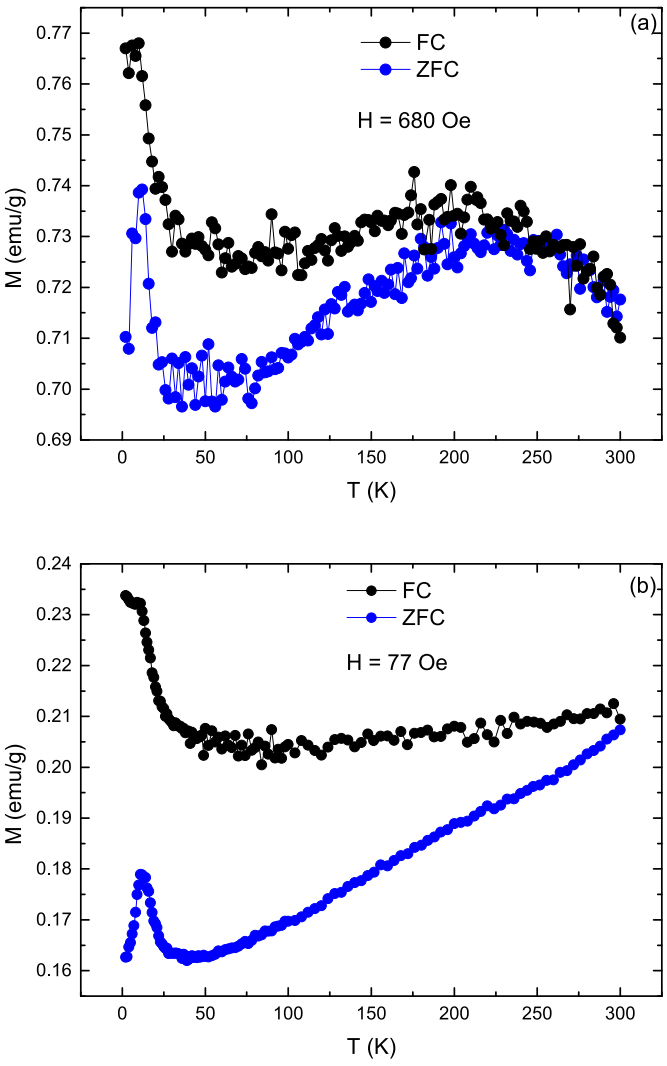

Fig. 3. ZFC and FC magnetization curves for samples (a) S10 and (b) S20. The applied magnetic fields of 680 Oe and 77 Oe for samples S10 and S20, respectively.

fitting of a standard sample of LaB_6 (SMR 660a). The peak profiles were fitted using the modified Thomson-Cox-Hasting formulation of the pseudo-Voigt function (TCHpV function). The Gaussian (H_G) and Lorentzian (H_L) contributions to the full width at half maximum of TCHpV function are given by:

$$H_G^2 = U\,tan^2\,\theta + V\,tan\,\theta + W + \frac{I_G}{cos^2\,\theta} \quad (1)$$

$$H_L = X\,tan\,\theta + \frac{Y}{cos\,\theta} \quad (2)$$

For both samples S10 and S20, the best fit was achieved considering $U = V = W = I_G = 0$, that is, a pure Lorentzian contribution to the diffraction line profile of NiO phase, while for sample S25 it was assumed $V = W = I_G = X = 0$ for the NiO phase, with the diffraction line profile describing Gaussian and Lorentzian contributions. For the Ni phase of all samples it was considered only a Lorentzian contribution to the diffraction line profile and no strain ($X = 0$). So the refinable profile parameters for samples S10 and S20 were X and Y for NiO phase and Y for Ni phase, respectively. Whereas for sample S25, the refinable profile parameters were U and Y for NiO phase and Y for Ni phase, respectively. This shows that X-ray line profile of NiO phase in the sample S25 is affected when a significant increase of Ni phase fraction occurs. The

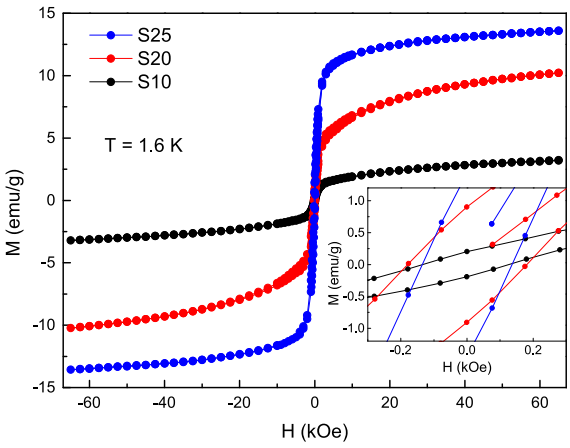

Fig. 4. (a) Magnetization vs. applied magnetic field for samples S10, S20, and S25 measured at 1.6 K. Inset shows M-H hysteresis loops for the lower field range.

crystallite size value for NiO phase of the sample S10 changes significantly from those of the samples S20 and 25, however the crystallite size values for Ni phase increases from sample S10 to sample S25. The microstrain of the NiO phase for sample S25 presented quite different value of those for samples S10 and S20. The microstrain increase for sample S25 can be caused by grain boundary between grains of Ni and NiO phases besides lattice defects. Thus, it should be noted that the microstructure properties of NiO phase are influenced by the increase of Ni phase percentage. The obtained results from X-ray line profile analysis are also listed in Table 2.

3.2. Morphological characterization by SEM

Fig. 2 shows the SEM micrographs for samples S10, S20 and S25, with magnification of 10.000×, 40.000X and 21.000X, respectively. We can observe, for the S10 sample, that particles aggregated to form large agglomerates with average size of about 3 μm with a pyramid-like shapes (Fig. 2a). For S20 and S25 samples, we verified that particles also aggregates but with a small average agglomerates size of about 130 nm and with a hexagonal surface morphology (Fig. 2b-c). However, the SEM analysis indicated a more regular distribution of particles of the same size for the S20 sample than for S25. Therefore, we showed that using different amounts of sorbitol in the synthesis of Ni/NiO systems implied in clear changes of the shape and size of S10, S20 and S25 samples, which also led to changes in the magnetic proprieties of Ni/NiO samples. The effect of chelating agent amount on the particle size was reported in the sol-gel synthesis of $LiMn_2O_4$ nanopowders using gelatin as chelating agent [21].

3.3. Magnetization

The temperature dependence of the zero-field cooling (ZFC) and field cooling (ZFC) magnetization (ZFC-FC M(T) curves) were measured in the temperature range of 2–300 K and plots are shown in Fig. 3. For sample S10, the behavior of the ZFC and FC magnetization curves as a function of temperature are fairly similar. We can observe that the ZFC and FC M(T) curves show irreversibility below 225 K, for an applied magnetic field of 680 Oe. ZFC magnetization shows a sharp peak at 12 K and a broad peak at 220 K, while in the FC magnetization an anomaly is observed below 10 K and the broad peak appears at 200 K. The sharp peak at low temperature can be related to a freezing temperature (T_f) of the uncompensated spins at the surface of the NiO particles. The broad peak at higher temperatures is associated with a blocking temperature (T_B) of a wide distribution of larger size nanoparticles. The S10 sample presents a low Ni fraction, so the major contribution to ZFC-FC magnetization behavior is due to the NiO fraction. Actually, the ZFC-FC magnetization features presented by sample S10 are similar to those observed in systems of NiO nanoparticles [22,23]. The ZFC-FC measurements for the S20 sample were carried out under application of a magnetic field of 77 Oe. The separation between the ZFC and FC magnetization curves is noted in the whole temperature range. The ZFC magnetization decreases from 300 K down to 50 K, after which it increases exhibiting a sharp peak at 12 K followed by a decrease as the temperature is further lowered down to 2 K. Decreasing the temperature from 300 to 50 K the FC magnetization decreases slightly and after 50 K it increases exhibiting an anomaly around 9 K. In comparison with data of sample S10 the ZFC and FC magnetization of the sample S20 exhibits a quite different behavior due to the increase of Ni phase at the expense of the NiO phase.

Table 3
Magnetic parameters for the Ni/NiO samples.

Sample	M_{65kOe} (emu/g)	M_R (emu/g)	H_C (Oe)
S10	3.19	0.20197	114
S20	10.2	0.90031	181
S25	13.6	1.4309	122

Magnetization as a function of applied magnetic field (M-H hysteresis loop) was measured at 1.6 K after the samples are zero-field cooled, in order to compare the magnetic properties of the obtained Ni/NiO samples.

M-H hysteresis loops in the range of −65 kOe to 65 kOe, for all three samples, are shown in Fig. 4. The magnetic hysteresis loops of the samples exhibit a weak ferromagnetic contribution, but no saturation was observed even at high applied magnetic field of 65 kOe. The ferromagnetic like behavior can be attributed to the Ni phase and the no saturation is due to the antiferromagnetic contribution of NiO phase [24]. The increase of the ferromagnetic Ni phase fraction in the samples can be accompanied by the rise of the magnetization value at 65 kOe from sample S10 to S25. Similar behavior has been observed in other Ni/NiO systems [25,26] and NiO based composites, in which the NiO amount was decreased and the ferrimagnetic phase content raises proportionally [27]. The magnetic parameters, such as magnetization at 65 kOe (M_{65kOe}), remnant magnetization (M_R) and coercivity (H_C) were obtained from magnetic hysteresis loops and they were listed in Table 3. The M_{65kOe} and M_R values differ considerably between samples. The S20 presented the highest coercivity among the samples, while the coercivity for S10 and S25 are relatively close.

4. Conclusion

The structural characterization results, XRD patterns, Rietveld refinement, and SEM, showed that polycrystalline Ni/NiO samples, with different phase proportions, were produced successfully by a sorbitol-based synthesis route. It found that the Ni phase percentage increased as the amount of sorbitol rose, which indicated that sorbitol played a important role in the synthesis process. We observed an increase of the saturation and remanent magnetization with increasing of the ferromagnetic Ni phase fraction in the samples. Therefore, this work shows that different amounts of sorbitol, used in the synthesis of Ni/NiO systems, imply in changes in the synthesized samples, surface morphologies, and magnetic properties.

Author contribution statements

C.M.R.R. prepared the samples and performed the XRD measurements. L.N. and W.P.Jr. carried out and analyzed the SEM micrographs. A.J.F.C. performed the Rietveld refinement. X.G. and V.A.C. carried out the magnetic measurements. X.G., V.A.C. and A.J.F.C. analyzed the magnetic measurements. A.J.F.C., W.P.Jr. and V.A.C. wrote the manuscript.

Declaration of competing interest

The authors declare that they have no known competing financial interests or personal relationships that could have appeared to influence the work reported in this paper.

Acknowledgments

All authors acknowledge supporting from the Brazilian agencies CAPES and CNPq. In addition, the authors acknowledge the use of the XRD and SEM facilities at LABNANO-AMAZON/UFPA. In particular, L. Nascimento and W. Paschoal Jr. gratefully acknowledge financial supporting from MAI/MCTIC/CNPq, PROPESP/UFPA and NanoJovem/PROEX/UFPA. Support from CNPq (grant 306715/2018-0) and FAPESP (07/56231-0; grant 2015/16191-5) is gratefully acknowledged.

References

[1] P.K. Manna, S.M. Yusuf, Two interface effects: exchange bias and magnetic proximity, Phys. Rep. 535 (2) (2014) 61–99, https://doi.org/10.1016/j.physrep.2013.10.002. http://www.sciencedirect.com/science/article/pii/S0370157313003773.

[2] F. Yuan, Y. Ni, L. Zhang, S. Yuan, J. Wei, Synthesis, properties and applications of flowerlike Ni–NiO composite microstructures, J. Mater. Chem. A 1 (29) (2013) 8438–8444, https://doi.org/10.1039/C3TA11219E, doi:10.1039/C3TA11219E.

[3] P. Ravikumar, D. Taparia, P. Alagarsamy, Thickness-dependent thermal oxidation of Ni into NiO thin films, J. Supercond. Nov. Magnetism 31 (11) (2018) 3761–3775, https://doi.org/10.1007/s10948-018-4651-6, doi:10.1007/s10948-018-4651-6.

[4] S. D'Addato, M.C. Spadaro, P. Luches, V. Grillo, S. Frabboni, S. Valeri, A. M. Ferretti, E. Capetti, A. Ponti, Controlled growth of Ni/NiO core–shell nanoparticles: structure, morphology and tuning of magnetic properties, Appl. Surf. Sci. 306 (2014) 2–6, https://doi.org/10.1016/j.apsusc.2014.02.060. http://www.sciencedirect.com/science/article/pii/S0169433214003535.

[5] A. Kremenović, B. Jančar, M. Ristić, M. Vučinić-Vasić, J. Rogan, A. Pačevski, B. Antić, Exchange-bias and grain-surface relaxations in nanostructured NiO/Ni induced by a particle size reduction, J. Phys. Chem. C 116 (7) (2012) 4356–4364, https://doi.org/10.1021/jp206658v, 10.1021/jp206658v.

[6] J. Livage, F. Beteille, C. Roux, M. Chatry, P. Davidson, Sol–gel synthesis of oxide materials, Acta Mater. 46 (3) (1998) 743–750, https://doi.org/10.1016/S1359-6454(97)00255-3.

[7] F. Fievet, J.P. Lagier, M. Figlarz, Preparing monodisperse metal powders in micrometer and submicrometer sizes by the polyol process, MRS Bull. 14 (12) (1989) 29–34, https://doi.org/10.1557/S0883769400060930.

[8] A.E. Danks, S.R. Hall, Z. Schnepp, The evolution of 'sol–gel' chemistry as a technique for materials synthesis, Mater. Horiz. 3 (2) (2016) 91–112, https://doi.org/10.1039/C5MH00260E, doi:10.1039/C5MH00260E.

[9] P.-Y. Silvert, R. Herrera-Urbina, N. Duvauchelle, V. Vijayakrishnan, K.T. Elhsissen, Preparation of colloidal silver dispersions by the polyol process. Part 1–Synthesis and characterization, J. Mater. Chem. 6 (4) (1996) 573–577, https://doi.org/10.1039/JM9960600573, doi:10.1039/JM9960600573.

[10] L. Poul, N. Jouini, F. Fiévet, Layered hydroxide metal acetates (metal = zinc, cobalt, and nickel): elaboration via hydrolysis in polyol medium and comparative study, Chem. Mater. 12 (10) (2000) 3123–3132, https://doi.org/10.1021/cm991179j, doi:10.1021/cm991179j.

[11] S.F. Shaikh, R.S. Mane, B.K. Min, Y.J. Hwang, O.-s. Joo, D-sorbitol-induced phase control of TiO_2 nanoparticles and its application for dye-sensitized solar cells, Sci. Rep. 6 (1) (2016) 20103, https://doi.org/10.1038/srep20103, doi:10.1038/srep20103.

[12] N. Priyadharsini, P.R. Kasturi, A. Shanmugavani, S. Surendran, S. Shanmugapriya, R.K. Selvan, Effect of chelating agent on the sol-gel thermolysis synthesis of $LiNiPO_4$ and its electrochemical properties for hybrid capacitors, J. Phys. Chem. Solid. 119 (2018) 183–192, https://doi.org/10.1016/j.jpcs.2018.03.004. http://www.sciencedirect.com/science/article/pii/S0022369717324629.

[13] V.A. Kochemirovsky, L.S. Logunov, S.V. Safonov, I.I. Tumkin, Y.S. Tver'yanovich, L.G. Menchikov, Sorbitol as an efficient reducing agent for laser-induced copper deposition, Appl. Surf. Sci. 259 (2012) 55–58, https://doi.org/10.1016/j.apsusc.2012.06.085. http://www.sciencedirect.com/science/article/pii/S0169433212011488.

[14] B.L. Cushing, V.L. Kolesnichenko, C.J. O'Connor, Recent advances in the liquid-phase syntheses of inorganic nanoparticles, Chem. Rev. 104 (9) (2004) 3893–3946, https://doi.org/10.1021/cr030027b, doi:10.1021/cr030027b.

[15] V. Ganeshchandra Prabhu, P.S. Shajira, N. Lakshmi, M. Junaid Bushiri, Magnetic properties of Ni/NiO nanocomposites synthesized by one step solution combustion method, J. Phys. Chem. Solid. 87 (2015) 238–243, https://doi.org/10.1016/j.jpcs.2015.09.001. https://www.sciencedirect.com/science/article/pii/S002236971530055X.

[16] M.S. Alnarabiji, O. Tantawi, A. Ramli, N.A. Mohd Zabidi, O.B. Ghanem, B. Abdullah, Comprehensive review of structured binary Ni-NiO catalyst: synthesis, characterization and applications, Renew. Sustain. Energy Rev. 114 (2019) 109326, https://doi.org/10.1016/j.rser.2019.109326. http://www.sciencedirect.com/science/article/pii/S1364032119305349.

[17] J. Rodríguez-Carvajal, Recent advances in magnetic structure determination by neutron powder diffraction, Physica B 192 (1) (1993) 55–69, https://doi.org/10.1016/0921-4526(93)90108-I. http://www.sciencedirect.com/science/article/pii/092145269390108I.

[18] M. Feygenson, A. Kou, L.E. Kreno, A.L. Tiano, J.M. Patete, F. Zhang, M.S. Kim, V. Solovyov, S.S. Wong, M.C. Aronson, Properties of highly crystalline NiO and Ni nanoparticles prepared by high-temperature oxidation and reduction, Phys. Rev. B 81 (1) (2010) 14420, https://doi.org/10.1103/PhysRevB.81.014420. https://link.aps.org/doi/10.1103/PhysRevB.81.014420.

[19] M. Thakur, M. Patra, S. Majumdar, S. Giri, Influence of cooling field on the magnetic properties of Ni/NiO nanostructure, J. Alloys Compd. 480 (2) (2009) 193–197, https://doi.org/10.1016/j.jallcom.2009.01.128. http://www.sciencedirect.com/science/article/pii/S0925838809002163.

[20] J. Rodríguez-Carvajal, T. Roisnel, Line broadening analysis using FullProf*: determination of microstructural properties, in: European Powder Diffraction EPDIC 8, Vol. 443 of Mater. Sci. Forum, Trans Tech Publications Ltd, 2004, pp. 123–126. https://doi.org/10.4028/www.scientific.net/MSF.443-444.123.

[21] N. Azad, H. Arabi, S.R. Ghorbani, A. Davodi, The effect of gelatin as a chelating agent on the synthesis and characterization of $LiMn_2O_4$ nanopowders prepared via sol–gel method, J. Sol. Gel Sci. Technol. 88 (2) (2018) 465–473, https://doi.org/10.1007/s10971-018-4833-5, doi:10.1007/s10971-018-4833-5.

[22] M. Jagodič, Z. Jagličić, A. Jelen, J.B. Lee, Y.-M. Kim, H.J. Kim, J. Dolinšek, Surface-spin magnetism of antiferromagnetic NiO in nanoparticle and bulk morphology, J. Phys. Condens. Matter 21 (21) (2009) 215302, https://doi.org/10.1088/0953-8984/21/21/215302.

[23] S. Thota, J. Kumar, Sol–gel synthesis and anomalous magnetic behaviour of NiO nanoparticles, J. Phys. Chem. Solid. 68 (10) (2007) 1951–1964, https://doi.org/10.1016/j.jpcs.2007.06.010. http://www.sciencedirect.com/science/article/pii/S0022369707002818.

[24] X. He, Y. Xu, X. Yao, C. Zhang, Y. Pu, X. Wang, W. Mao, Y. Du, W. Zhong, Large exchange bias and enhanced coercivity in strongly-coupled Ni/NiO binary nanoparticles, RSC Adv. 9 (52) (2019) 30195–30206, https://doi.org/10.1039/C9RA03242H, doi:10.1039/C9RA03242H.

[25] L. Del Bianco, F. Boscherini, A.L. Fiorini, M. Tamisari, F. Spizzo, M.V. Antisari, E. Piscopiello, Exchange bias and structural disorder in the nanogranular Ni/NiO system produced by ball milling and hydrogen reduction, Phys. Rev. B 77 (9) (2008) 94408, doi:10.1103/PhysRevB.77.094408, https://link.aps.org/doi/10.1103/PhysRevB.77.094408.

[26] S. Kar, V. Singh, Structural investigations of oxidative behavior on nanocrystalline nickel, J. Alloys Compd. 509 (8) (2011) 3582–3586, https://doi.org/10.1016/j.jallcom.2010.12.077. http://www.sciencedirect.com/science/article/pii/S0925838810030690.

[27] A.J. Freitas Cabral, J.P. Serna, B.R. Salles, M.A. Novak, A.L. Pinto, C.M. R. Remédios, Exchange bias effect in polycrystalline $NiO/NiMn_2O_4$ composite, J. Alloys Compd. 630 (2015) 74–77, https://doi.org/10.1016/j.jallcom.2014.12.179. http://www.sciencedirect.com/science/article/pii/S0925838814031077.